



Contents lists available at ScienceDirect

Experimental Eye Research

journal homepage: www.elsevier.com/locate/yexerVisual cycle modulation in neurovascular retinopathy[☆]James D. Akula^{a,b}, Ronald M. Hansen^{a,b}, Radouil Tzekov^{c,1}, Tara L. Favazza^a, Tanya C. Vyhovskiy^a, Ilan Y. Benador^a, Julie A. Mocko^a, David McGee^{c,2}, Ryo Kubota^{c,**}, Anne B. Fulton^{a,b,*}^a Department of Ophthalmology, Children's Hospital Boston, Boston, MA, USA^b Department of Ophthalmology, Harvard Medical School, Boston, MA, USA^c Acucela Inc., 21720 23rd Dr. SE, Suite 120, Bothell, WA 98021-3906, USA

ARTICLE INFO

Article history:

Received 21 December 2009

Accepted in revised form 18 April 2010

Available online xxx

Keywords:

retinopathy
electroretinography
visual cycle
metabolism
photoreceptors
retinoid
N-retinylacetamide

ABSTRACT

Rats with oxygen-induced retinopathy (OIR) model the pediatric retinal disease retinopathy of prematurity (ROP). Recent findings in OIR rats imply a causal role for the rods in the ROP disease process, although only experimental manipulation of rod function can establish this role conclusively. Accordingly, a visual cycle modulator (VCM) – with no known direct effect on retinal vasculature – was administered to “50/10 model” OIR Sprague–Dawley rats to test the hypotheses that it would 1) alter rod function and 2) consequently alter vascular outcome. Four litters of pups ($N = 46$) were studied. For two weeks, beginning on postnatal day (P) 7, the first and fourth litters were administered 6 mg kg⁻¹ N-retinylacetamide (the VCM) intraperitoneally; the second and third litters received vehicle (DMSO) alone. Following a longitudinal design, retinal function was assessed by electroretinography (ERG) and the status of the retinal vessels was monitored using computerized fundus photograph analysis. Rod photoreceptor and post-receptor response amplitudes were significantly higher in VCM-treated than in vehicle-treated rats; deactivation of phototransduction was also significantly more rapid. Notably, the arterioles of VCM-treated rats showed significantly greater recovery from OIR. Presuming that the VCM did not directly affect the retinal vessels, a causal role for the neural retina – particularly the rod photoreceptors – in OIR was confirmed. There was no evidence of negative alteration of photoreceptor function consequent to VCM treatment. This finding implicates the rods as a possible therapeutic target in neurovascular diseases such as ROP.

© 2010 Elsevier Ltd. All rights reserved.

1. Introduction

Abnormal retinal function is a feature of neovascular retinal diseases such as retinopathy of prematurity (ROP). Thus, these diseases could also be classified as neurovascular diseases (Fulton et al., 2009a). The clinical hallmark of high-risk ROP (“plus disease”) is the appearance of tortuous and dilated vessels at the posterior pole of the eye (ETROP, 2003). Notably, the appearance of the vascular abnormalities that characterize acute ROP, including tortuosity and neovascularization (NV), is coincident with the period of developmental elongation of the rod photoreceptors’ outer segments and the accompanying increase in retinal rhodospin

content (Dembinska et al., 2002; Fulton et al., 1991, 1995, 1999a, 2009b; Luty et al., 2006; Palmer et al., 1991). Data from one rat model of ROP (Reynaud and Dorey, 1994; Reynaud et al., 1995) show that rod photoreceptor dysfunction antedates the appearance of both vascular tortuosity and NV, while data from another rat model show that rod photoreceptor sensitivity at an early age predicts the severity of the vascular tortuosity at adult ages (Akula et al., 2007). Thus, despite the fact that abnormalities in the morphology of the retinal vessels are the main diagnostic criterion, ROP may be first a disorder of the neural retina with secondary vasculopathy.

Vascular endothelial growth factor mediates retinal vessel tortuosity (Akula et al., 2008; Hartnett et al., 2008) and is upregulated by local hypoxia (Pe'er et al., 1995; Shweiki et al., 1992). Therefore, the oxygen demands of the retina might underpin the development of tortuous vessels in ROP (Arden et al., 2005). Thus, it is not surprising that in ROP there is a significant association of visual outcome, function of the neural retina, and severity of blood vessel abnormalities (Fulton and Hansen, 1995; Good, 2004).

Of the retinal cells, the rods have by far the highest oxygen demands (Cringle et al., 1991). This is because they perform three (linked) metabolically demanding processes: generation of the dark current, the visual (retinoid) cycle, and outer segment

[☆] Supported by Acucela Inc., the March of Dimes Birth Defect Foundation, the Massachusetts Lions Eye Research Fund, and the Pearle Vision Foundation.

* Corresponding author at: Children's Hospital Boston, 300 Longwood Ave., Fegan 4, Boston, MA 02115-5724, USA. Tel.: +1 617 355 5685; fax: +1 617 738 8178.

** Corresponding author. Tel.: +1 425 527 3260.

E-mail addresses: rkubota@acucela.com (R. Kubota), anne.fulton@childrens.harvard.edu (A.B. Fulton).

¹ Current address: Department of Ophthalmology, University of Massachusetts Medical School, Worcester, MA, USA.

² Current address: MPI research, Mattawan, MI, USA.

turnover, all of which ensue concomitant to developmental elongation of their outer segments (ROS) and the increase of retinal rhodopsin content. The signal transduction mechanism of the rods is physiologically unique. In darkness, sodium and other cations intruded through cyclic guanosine monophosphate (cGMP) gated channels in the ROS are expelled by pumps in the rod inner segment so rapidly that a volume equal to the entire cytosol is circulated every half minute (Hagins et al., 1989). The molecular cascade initiated by photon capture at rhodopsin following a flash of light and leading to a reduction of cGMP leads the dark current to decay following the form of a delayed Gaussian that can be described by an intrinsic amplification constant, A (Lamb and Pugh, 1992; Pugh and Lamb, 1993). Following photon capture, rhodopsin's chromophore (retinol) undergoes an isomeric change which frees it from opsin and initiates phototransduction. Spent chromophore is passed from the ROS to the retinal pigment epithelium (RPE) where it undergoes a series of transformations before being returned to the ROS through the apical processes of the RPE as retinol. There it becomes covalently linked to its active-site lysine in opsin, becoming rhodopsin again and completing the visual cycle (Kuksa et al., 2003; McBee et al., 2001; Rando, 2001). The rate-limiting step in the visual cycle is mediated by the isomerase enzyme complex, RPE65 (Moiseyev et al., 2005). Other byproducts of phototransduction in the ROS are expelled through a process of circadian shedding of the ROS tips; each RPE cell phagocytizes thousands of disks shed from 30 to 50 embedded rods each day (Young, 1967).

Substances that alter one of these fundamental functions of immature rods but have no direct effect on retinal vasculature could serve to test the hypothesis that the rods contribute to the onset of vasculopathy in ROP; these substances might also have therapeutic application as neuroprotectors (Fulton et al., 2009a; Travis et al., 2007). Controlled down-regulation of the visual cycle through targeted inhibition of RPE65 activity lowers the flux of retinoids through the ROS/RPE complex, presumably rendering the rods less vulnerable to insult from hyperoxia and hypoxia (Wellard et al., 2005) by reducing their metabolic demands. It might also reduce the accumulation of misfolded proteins, slowing phagocytosis, and therefore lengthen the ROS. And, since the early status of the rods predicts blood vessel tortuosity at older ages (Akula et al., 2007), blood vessel outcomes might consequently be altered.

Rat models of ROP provide a convenient *in vivo* system in which the relation of the photoreceptors to the retinal vasculature can be studied and manipulated. Visual cycle modulation (VCM) was first shown to exhibit neuroprotective properties in a rat light damage model (Sieving et al., 2001). *N*-retinylacetamide is a non-carotenoid, vitamin-A derivative, (VCM see appendix) that alters, seemingly reversibly, the function of the rod photoreceptors: Messias et al. (2010) report that single administrations of this VCM induce, in healthy adult rats, electroretinographic (ERG) changes consistent with a decrease in the rate of 11-*cis*-retinal regeneration. For instance, a few hours after a single administration of the VCM, the amplitude of the ERG *b*-wave response is, relative to sham, normal in the dark-adapted eye but greatly reduced for more than 60 min following a partial bleach. These differences are no longer detectable a few weeks later.

Hereinafter, the effects of *N*-retinylacetamide on rats with an oxygen-induced retinopathy (OIR) that models human ROP are described.

2. Materials and methods

2.1. Experimental design

Retinopathy was induced in four litters of Sprague–Dawley rat pups ($N = 46$) by exposing them to alternating 24 h periods of

$50 \pm 1\%$ and $10 \pm 1\%$ oxygen from the day of birth to postnatal day (P) 14 (Penn et al., 1994, 1995), as shown in Fig. 1. The light cycle was 12 h 10–30 lux and 12 h dark, except during test days when constant darkness was maintained. The light-to-dark transition coincided with each oxygen alternation. Once per day for two weeks, beginning on P7, at the time of the oxygen level change and the light-to-dark transition, the first and fourth litters were injected intraperitoneally with 6 mg kg^{-1} *N*-retinylacetamide (see Appendix for details); the second and third litters received an equivalent volume of vehicle (20% dimethyl sulfoxide, DMSO) alone. The injection schedule was designed to continue over the age range that begins with the onset of rapid increase in the rhodopsin content of the retina and lasts until rhodopsin content exceeds 50% of its adult amount (Fulton and Baker, 1984). The dose was selected because studies in mouse suggested it would suppress the visual cycle by approximately 50% (see Appendix). The injection process resulted in the rats being held in room air (20.8% oxygen) for approximately 20 min between each oxygen alternation. The rats were assessed, following a longitudinal design, with tests at P20–22, P30–32, and P60–62. These ages capture the height of vascular abnormality, a period of marked recovery, and an adult age, respectively (Akula et al., 2007; Liu et al., 2006). At each test age, the function of the neural retina and the morphology of the retinal vasculature were evaluated using noninvasive techniques, specifically ERG and semi-automated computerized analysis of the blood vessels captured in digital fundus photographs (Martinez-Perez et al., 2002, 2007). All experiments were conducted according to the ARVO Statement for the Use of Animals in Ophthalmic and Vision Research and with the approval of the Animal Care and Use Committee at Children's Hospital Boston.

2.2. Electroretinography

2.2.1. Calibration of light flashes

ERG stimuli were delivered using an Espion e^2 with ColorDome Ganzfeld stimulator (Diagnosys LLC, Lowell, MA). The rate of photoisomerization per rod (R^*) for the green LED flash was calculated by measuring the flux density incident upon an integrating radiometer (IL1700; International Light, Newburyport, MA) positioned at the location of the rat's cornea, and following the procedures detailed by Lyubarsky and Pugh (1996). The LED was treated as

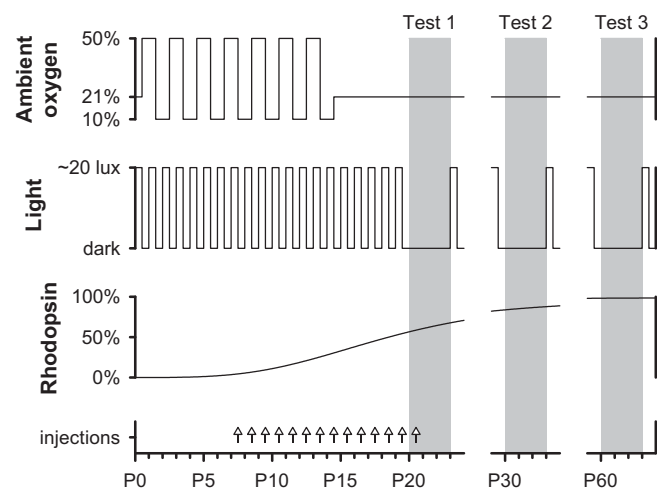


Fig. 1. Key features of the experimental paradigm. The ambient oxygen and light cycle were tightly controlled and synchronized. Dosing with the VCM (*N*-retinylacetamide) was designed to target the rapid growth phase of the developmental increase in rhodopsin in the retina (arrows). Grey bars indicate the three test windows.

monochromatic with λ equal to 530 nm. The intensity of the flash was given by

$$i(\lambda) = Q(\lambda) \cdot T(\lambda) \cdot \frac{a_{\text{pupil}}}{a_{\text{retina}}} \cdot a_{\text{rod}}(\lambda) \quad (1)$$

where $i(\lambda)$ is R^* , $Q(\lambda)$ is the calculated photon density at the cornea, $T(\lambda)$ is the transmissivity of the ocular-media and pre-receptor retina ($\sim 80\%$ at 530 nm; [Alpern et al., 1987](#)), and a_{pupil} , a_{retina} and $a_{\text{rod}}(\lambda)$ are respective estimates of the area of the dilated pupil $\sim \text{mm}^2$; [Dodt and Echte, 1961](#)), the area of the retinal surface ($\sim 50 \text{ mm}^2$; [Hughes, 1979](#)), and the end-on light collecting area of the rod photoreceptor ($\sim 1.5 \mu\text{m}^2$ at 530 nm). $a_{\text{rod}}(\lambda)$ takes into account the length of the outer segment, the absorption spectrum of the rod, and the optical density of the photopigment, as well as the radius of the photoreceptor ([Baylor et al., 1979](#)). Since several of these parameter values are unknown for the rat rod that is affected by OIR, stimuli are expressed as the expected values in adult control rats. $Q(\lambda)$ was found by

$$Q(\lambda) = \lambda \cdot \frac{P_\lambda}{h \cdot c} \quad (2)$$

where P_λ is the radiant flux (W), h is Planck's constant and c is the speed of light ([Wyszecki and Stiles, 1982](#)). To evaluate the intensity of 'white' xenon-arc flashes, an intensity series with interspersed green and white flashes was recorded and the equivalent light was estimated based on the shift of the stimulus/response curves for the scotopic b -wave.

2.2.2. Calibration of the bleaching light

The bleach was produced using an Ektagraphic III B slide projector (Eastman Kodak, Rochester, NY) with an EXR 300 W halogen lamp (color temperature 3350). To diffuse the light, a hemisected Ping-Pong ball was placed over the eye. The projector was positioned on a platform so that its lens was approximately 6 cm from the surface of the ball. The power of the light was measured using the radiometer, with the integration feature turned off, positioned under the Ping-Pong ball at the location of the rats' head. The calculation of the number of photons incident upon the photodetector ($\text{quanta cm}^{-2} \text{ s}^{-1}$) was calculated using eq. (2) and assuming $\lambda = 500 \text{ nm}$. The strength of the bleach was estimated by

$$R_0(t) = \exp\left(-\frac{Q(\lambda) \cdot t}{Q_e}\right) \quad (3)$$

where $1 - R_0$ is the fraction of rhodopsin bleached at the termination of the light exposure, t is the duration (60 s) of the exposure, and Q_e (quanta cm^{-2}), the inverse of photosensitivity, is the energy needed to leave $1/e$ of rhodopsin unbleached ([Perlman, 1978](#)). Earlier measurements indicate that the value of Q_e in Sprague–Dawley rats is approximately $15.8 \log \text{quanta cm}^{-2}$ ([Fulton and Baker, 1984](#)). Thus, the light, which produced approximately $15.9 \log \text{quanta cm}^{-2}$, bleached $\sim 60\%$ of the rhodopsin in the retina.

2.2.3. Preparations

Dark-adapted subjects were anesthetized with a loading dose of approximately 75 mg kg^{-1} ketamine and 8 mg kg^{-1} xylazine, injected intraperitoneally. This was followed by a booster dose (50% of loading dose) administered intramuscularly. The pupils were dilated with a combination of 1% phenylephrine hydrochloride and 0.2% cyclopentolate hydrochloride (Cyclomydril; Alcon, Fort Worth, TX). The corneas were anesthetized with one drop of 0.5% proparacaine hydrochloride. A Burian–Allen bipolar electrode (Hansen Laboratories, Coralville, IA) was placed on the cornea and the

ground electrode was placed on the tail. The red light was extinguished, and the animals remained in total darkness for an additional 10 min to allow them to return to a fully dark-adapted state before experimentation commenced.

2.2.4. The activation of phototransduction

At the first test date, animals were assigned half-hazard such that half of each litter (rounded up if odd in number) participated in studies of the activation and deactivation of phototransduction, and of post-receptor retinal function ($n = 24$: 12 VCM, 12 vehicle); the remainder participated in the bleaching experiments. As shown in [Fig. 2A](#), characteristics of the rod photoresponse were estimated from the ERG by fitting the parameters of the [Hood and Birch \(1992\)](#) formulation of the [Lamb and Pugh \(1992; Pugh and Lamb, 1993\)](#) model of the biochemical processes involved in the activation of phototransduction to the a -waves elicited by the five brightest flashes:

$$P_3(i, t) = Rm_{p3} \cdot (1 - \exp(-1/2 \cdot i \cdot S \cdot (t - t_d)^2)) \quad (4)$$

for $t_d < t < 20 \text{ ms}$.

In this model, i is the intensity of the flash (R^*) and t is elapsed time (s). The values of the free parameters in the model, Rm_{p3} , S , and t_d , were optimized using a routine (fmins; MATLAB R11, The Mathworks, Natick, MA) that minimizes the sum of squared deviates. Rm_{p3} is the amplitude (μV) of the saturated rod response; it is proportional to the magnitude of the dark current and depends upon the number of channels available for closure by light in the ROS ([Lamb and Pugh, 1992; Pugh and Lamb, 1993](#)), which, under normal conditions, in turn depends directly upon the length of the ROS ([Reiser et al., 1996](#)). S is a sensitivity ($R^*^{-1} \text{ s}^{-2}$) parameter that, if stimulus intensity is correctly specified, is related to the amplification constant, A , which summarizes the kinetics of the series of processes initiated by the photoisomerization of rhodopsin and resulting in closure of the channels in the plasma membrane of the photoreceptor. t_d is a brief delay (s). Fitting of the model was restricted to the leading edge of the a -wave.

2.2.5. The deactivation of phototransduction

In the same rats, using a double-flash paradigm, the time-course of the rod response to a 'green' ($\lambda_{\text{max}} \approx 530 \text{ nm}$) conditioning flash (CF) producing approximately $150 R^*$ was derived. This green flash, while eliciting an a -wave of less than half of the saturated rod response, was nevertheless sufficient to fully suppress the dark current. First, the response to the CF was recorded alone. Then, the amplitude of the response to an intense, rod-saturating (approximately $10,000 R^*$) 'white' xenon-arc probe flash (PF, *grey trace* in [Fig. 2A](#)) was determined. The amplitude of the PF response, a_{max} (μV), which was measured at 8 ms after presentation (just before the trough of the a -wave), was taken as proportional to the maximal rod dark current. Next, the CF and PF were presented together, separated by 10 predetermined inter-stimulus intervals (10 ms, 20 ms, 50 ms, 0.1 s, 0.15 s, 0.2 s, 0.4 s, 0.7 s, 1 s, and 1.4 s). In double-flash conditions, the response to the CF recorded alone served as the baseline for measuring the amplitude of the response to the PF at each inter-stimulus time t , $a_{\text{sat},t}$ ([Fig. 2B](#)). The proportion of the dark current suppressed by the CF at elapsed time t , SF_t , was, therefore, given by

$$SF_t = 1 - \frac{a_{\text{sat},t}}{a_{\text{max}}} \quad (5)$$

To derive a value for the time-course of deactivation ([Fig. 2C](#)), the trough of the rod response was determined and a line was fit

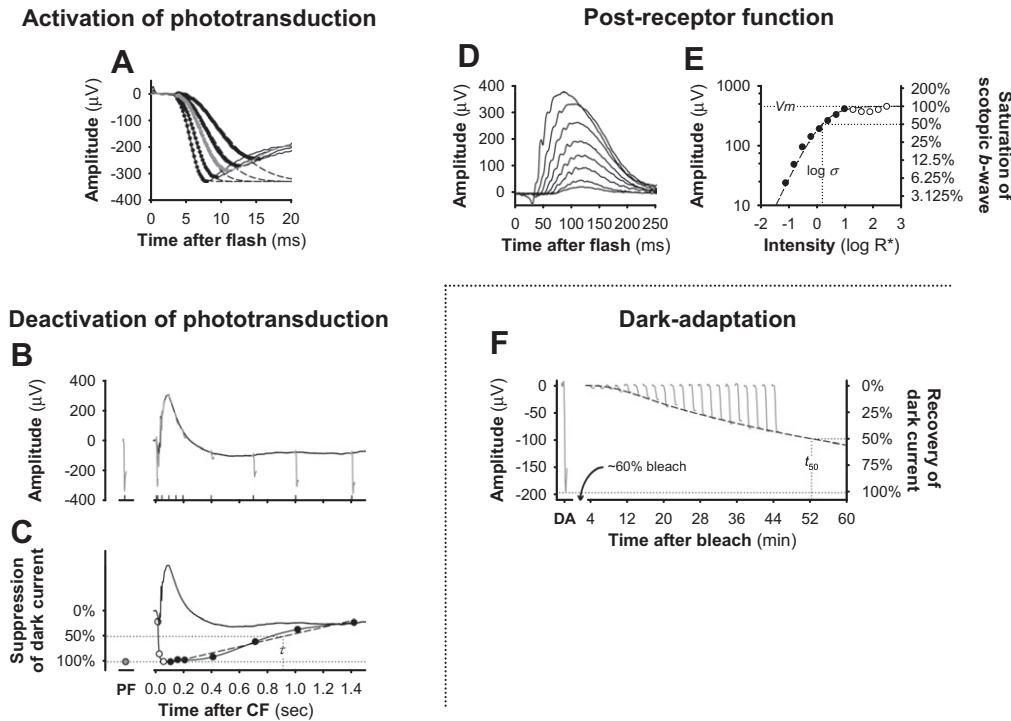


Fig. 2. Electrophysiological methods. Data in panels A–E were obtained from the same P30 VCM-treated rat. Data in panel F were obtained from a different, P30 VCM-treated rat. (A) Rod-saturating ERG records elicited with bright ‘white’ flashes (black or grey lines), and fits of the Hood and Birch formulation of the Lamb and Pugh model (eq. (4)) of the activation of phototransduction (dashes) to the leading edge of the *a*-wave (symbols). The flash eliciting the grey trace was subsequently used as a probe of the dark current; responses elicited by this probe flash (PF) are indicated in grey in panels B, C, and F. (B) The PF is presented at fixed intervals (ticks) after a ‘green’ conditioning flash (CF) to rapidly drive the rods to saturation, thus manifesting the constituent rod current. (C) Derivation of the time-course of the rod photoreponse to the CF. The time to 50% recovery, τ , is estimated by fit of a line (dashes) to the recovery phase of the photoresponse (filled symbols). (D) Scotopic ERG records elicited with ‘green’ flashes of doubling intensity. (E) The amplitudes of the ERG *b*-waves plotted as a function of log flash intensity. The Naka–Rushton function (eq. (6)) is fit through the *b*-wave amplitudes (circles) only to intensities before marked intrusion of the *a*-wave (filled symbols). The flash intensity producing half-maximal *b*-wave amplitude, $\log \sigma$, is indicated, as is the upper asymptotic value, V_m . (F) The PF is presented in the dark, and at 2 min intervals following a rhodopsin bleaching stimulus. The time to 50% recovery of the dark-adapted PF amplitude, t_{50} , is derived by fit of eq. (7).

through the recovery phase. The latency to 50% recovery, τ (ms), was noted.

2.2.6. Post-receptor function

Rod-mediated, post-receptor function was evaluated, in the same animals, from the ERG *b*-wave. A series of 13 ‘green’ flashes producing from approximately 0.075 to 300 R^* was used to elicit *b*-wave responses. Fig. 2D displays the first eight responses, including to that first intensity at which the *a*-wave is clearly visible. To the amplitudes (μV) of such responses, the parameters of the Naka–Rushton function,

$$\frac{V(i)}{V_m} = \frac{i}{i + \sigma}, \quad (6)$$

were optimized (Fig. 2E). In this equation, $V(i)$ is the amplitude of the response to a flash of i intensity (R^*), V_m is the saturated amplitude of the *b*-wave, and σ is the intensity that evokes a *b*-wave with amplitude of half V_m . As indicated by the filled circles in Fig. 2E, the function was fit only up to those intensities at which *a*-wave intrusion was first observed. Again, if i is correctly specified, $\log \sigma$ is a measure of post-receptor sensitivity.

2.2.7. Recovery from a bleach

In the second set of experiments, performed on cohorts ($n = 22$: 10 VCM, 12 vehicle), the recovery of the dark current from the bleach was assessed. As shown in Fig. 2F, the rod-saturating PF (10,000 R^*), presented to the dark-adapted eye, was used to

determine the magnitude of the dark current. Following the bleaching exposure, the response to the PF was monitored at 2 min intervals for approximately 40 min. At each time, the fraction of the dark current recovered ($1 - SF_t$) was calculated. The time to 50% recovery of the saturating rod photoreponse, t_{50} , was found by optimizing the parameters of the function

$$t(P) = -t_0 \cdot \ln\left(\frac{P - P_0}{B}\right) \quad (7)$$

and then solving the equation for $P = 50\%$. In this equation, $t(P)$ is the time required for the *a*-wave to reach P percent of its dark-adapted value, t_0 is the time constant of regeneration, P_0 is the normalized amplitude of the dark-adapted *a*-wave (100%), and B is a scalar. Often, t_{50} was longer than the recording session and was therefore extrapolated.

2.2.8. Stimulus delivery

The timing and intensity of the ERG stimuli were under computer control. The inter-stimulus interval and number of sweeps averaged for the intensity series used to assess receptor and post-receptor response sensitivities and amplitudes are detailed in Table 1. For the deactivation experiments, the response to the conditioning flash was averaged eight times, the response to the probe flash was averaged four times and, in double-flash conditions, all traces were averages of two sweeps, recorded 1 min apart. In the bleaching experiment, the probe flash was delivered singly every 2 min.

Table 1
ERG intensity series.

Light source	Intensity ^a (R ⁺)	Sweeps (minimum)	I.S.I. (s)
'Green' LED	0.075	32	0.35
	0.15	24	0.40
	0.30	24	0.45
	0.60	18	0.50
	1.0	18	0.60
	2.5	14	0.75
	5.0	14	1.0
	9.5	11	1.5
	20	11	2.0
	40	8	2.5
	75	8	4.0
	150	6	5.5
	300	6	8.0
Xenon-arc	1000	5	18
	2500	4	27
	5000	4	40
	10,000	3	60
	20,000	3	90

^a The efficiency (R⁺ cd⁻¹ s⁻¹ m²) of the 'green' LED and xenon-arc flashes were respectively calculated at ~150 and ~75.

2.3. Analysis of the retinal vessels

Vascular tortuosity was evaluated in both eyes of subjects using a noninvasive technique, a necessity in this longitudinal study. The OIR model employed in this study is characterized by a 100% incidence of NV (Akula et al., 2009; Barnett et al., 2009; Penn et al., 1995); it is also characterized by tortuous retinal vessels (Akula et al., 2007; Akula et al., 2008; Berkowitz et al., 2007; Hartnett et al., 2008; Liu et al., 2006). In patients, the posterior pole is the region most important to the diagnosis of high-risk ROP (ETROP, 2003). Correspondingly, following each ERG session, wide-field images of the ocular fundus showing the major vessels of the retina were obtained and composited to display a complete view of the posterior pole, defined here as the region within the circle bounded by the vortex veins and concentric to the optic nerve head; the vortex veins define the equator. The arterioles were identified and their tortuosity measured using RISA software, as previously

described (Akula et al., 2007; Akula et al., 2008; Gelman et al., 2005; Hansen et al., 2008; Martinez-Perez et al., 2002, 2007). Briefly, each vessel was cropped from the main image and segmented individually. If necessary, the segmented image was manually edited to remove extraneous features such as the background choroidal vasculature. RISA constructed a skeleton and marked terminal and bifurcation points. The user then selected the vessel segments for analysis and RISA automatically calculated the integrated curvature, *IC*, for the selected segments of each vessel. *IC* captures any departure from linear course and is the sum of angles along the vessel, normalized by the vessel length (radians pixel⁻¹). Thus, a theoretical straight vessel has *IC* = 0. High values of *IC* capture well vessels that a clinician would be likely to designate as tortuous (Gelman et al., 2005). Arteriolar tortuosity, *T_A* (radians pixel⁻¹), was calculated for each subject as the mean integrated curvature of all measurable arterioles in both eyes (median 10). In agreement with previous reports (Akula et al., 2007; Liu et al., 2006), the venules were little affected by the OIR.

3. Results

3.1. ERG

From records similar to those shown in Fig. 2A, rod response sensitivity (*S*) and saturating amplitude (*Rm_{P3}*) were obtained (eq. (4)) from VCM- and vehicle-treated rats. Analysis of variance (ANOVA) showed no statistically significant effect of VCM on *S* (Fig. 3A); on the other hand, *Rm_{P3}* was significantly (*p* < 0.001) increased in VCM-treated rats, most markedly at the P30–32 test (Fig. 3B). Deactivation of phototransduction (*τ*), assessed using the double-flash protocol, was significantly (*p* < 0.01) faster in VCM-treated rats (Fig. 3C). Bipolar cell response sensitivity (*log σ*) and saturating amplitude (*V_m*) were obtained from the *b*-wave stimulus response function (eq. (6)); *log σ* was not affected by VCM (Fig. 3D), but *V_m* was significantly (*p* < 0.01) increased in VCM rats (Fig. 3E), again most markedly at the P30 test.

The time to 50% recovery of the *a*-wave following the bleaching stimulus (*t₅₀*, eq. (4)) was assessed to determine if VCM adversely affected the regeneration of rhodopsin in the rods. *t₅₀* was not

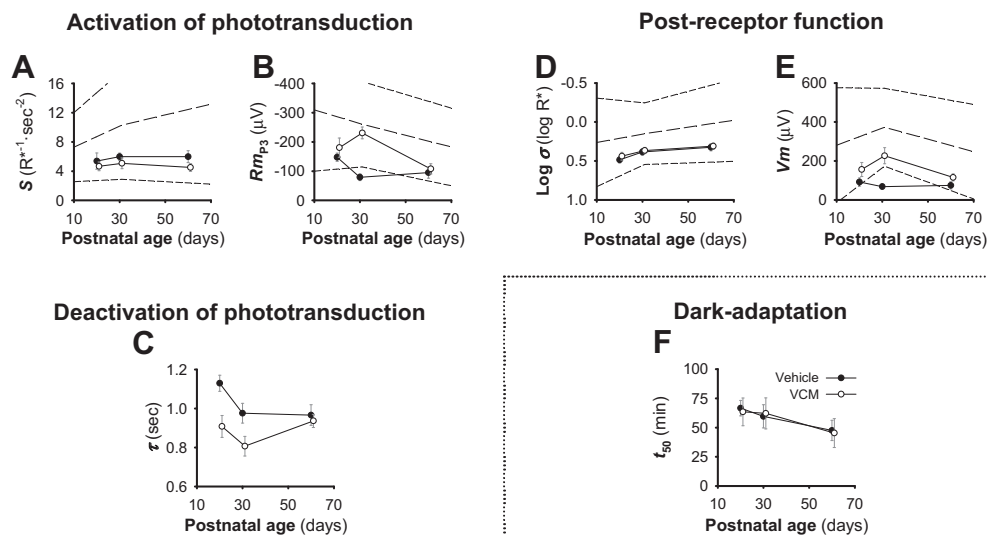


Fig. 3. Electrophysiological data (mean ± SEM); points are slightly offset on the age axis for clarity. The long and short dashed lines in panels A, B, D and E denote, respectively, the mean and 95% prediction interval for normal (Whitmore, 1986), room-air-reared rats, derived from previously published data (Akula et al., 2007, 2008; Liu et al., 2006). The key in panel F applies to all panels. (A) Rod sensitivity. (B) Amplitude of the saturated rod response. (C) Time constant of the deactivation of phototransduction. (D) Post-receptor sensitivity. (E) Amplitude of the saturated post-receptor response. (F) Time to 50% recovery from the bleach.

significantly altered by VCM and did not vary significantly with age (Fig. 2F).

3.2. Blood vessels

Sample outcome images (P60) for a VCM- and a vehicle-treated rat are shown in Fig. 4A, a and the arterioles, as segmented by RISA, are shown in Fig. 4B along with their corresponding IC values. From such analyses, mean arteriolar tortuosity (T_A) was calculated for each animal. ANOVA of T_A detected no significant main effect of VCM. However, a significant group \times age interaction ($p = 0.002$) indicated that T_A recovered more rapidly in VCM than vehicle-treated rats (Fig. 4C). To test this, the value of T_A at P20 was

subtracted from the value of T_A at P60 in each rat to determine the change in arteriolar tortuosity during the period of observation (Fig. 4D). An evaluation of these $\Delta P60$ –P20 data by t -test confirmed that VCM resulted in more than twice the normal amount of vascular recovery ($p = 0.001$).

4. Discussion

Rats that received *N*-retinylacetamide had larger rod and rod-mediated response amplitudes (Rm_{p3} , Vm) and faster recovery from transduction (τ) than rats that received only vehicle. This is evidence that VCM improved rod function, albeit transiently, without significant adverse effects.

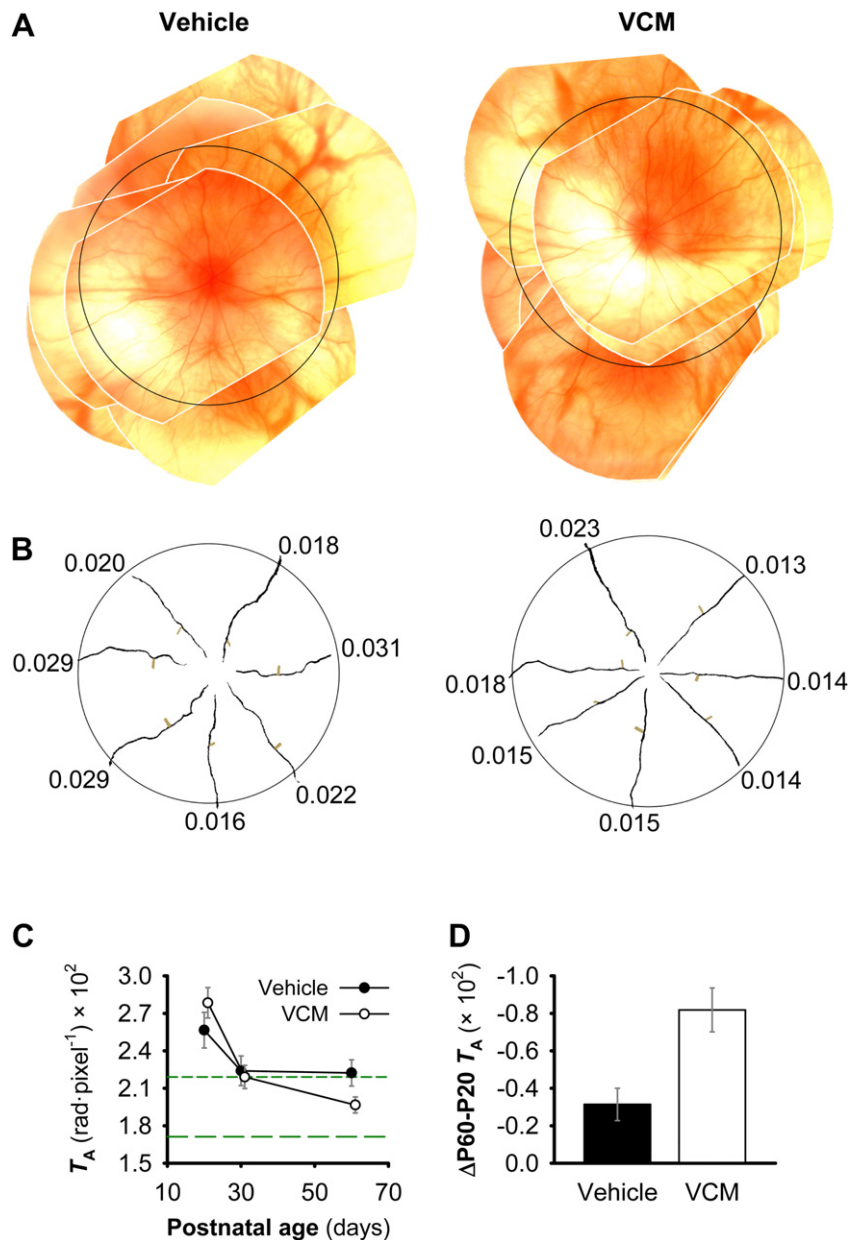


Fig. 4. Analysis of the retinal vasculature. (A) Sample composite fundus photographs from adult VCM- and vehicle-treated rats taken at the P60 test. The white borders were added to demark the boundaries of individual images and were not present in the original analysis of the retinal arterioles. The analysis was constrained to the posterior pole (black circle). (B) The arterioles as segmented by RISA (black segments). RISA requires a bifurcation, so for un-bifurcated vessels, one was drawn arbitrarily (tan segments), though these were irrelevant to the analysis. (C) Mean \pm SEM tortuosity of the retinal arterioles; points are slightly offset on the age axis for clarity. The long and short dashed green lines denote, respectively, the mean and upper 95% prediction limit for normal, room-air-reared rats, derived from previously published (Akula et al., 2007, 2008) and unpublished data (the lower limit is not shown). Note that the data are plotted at a gain of 100 (centiradians). (D) Mean \pm SEM change in T_A between first (P20–22) and last (P60–62) observations.

There are at least two explanations for the larger rod response (R_{mp3}) found in VCM-treated rats. One is lengthened ROS. If slowing the visual cycle resulted in less outer segment shedding, then the ROS would naturally elongate; this would have the effect of increasing the radial magnitude of the dark current. It would also serve to increase quantum efficiency of the rods, increasing the i term in eq. (4) and thus resulting in a proportionately lower calculated S , although not necessarily altering the underlying amplification constant, A . Changes in rod sensitivity were not significant but did trend lower at every age in the VCM rats (Fig. 3A). Rod response amplitudes in vehicle-treated rats were on the low end of the range of values previously observed (Akula et al., 2007, 2008; Liu et al., 2006) in this model, perhaps a consequence of DMSO retinal toxicity (Tsai et al., 2009). In VCM-treated rats, both rod and post-receptor (V_m) response amplitudes fell within the normal range at every age tested.

Another explanation is that the slowed visual cycle allowed the rods to form better organized outer segments, which are disorganized in some OIR models (Fulton et al., 1999b). Molecular movement (including of all-*trans*-retinal leaving the ROS) would be faster in well formed outer segments, and ion influx and efflux through the ROS membrane would be likewise improved. This could explain the reduction in τ in VCM-treated rats as, for example, calcium influx is critical to the inactivation of the rods' light response (Howes et al., 2002; Lyubarsky et al., 1996; Matthews and Fain, 2003). It might also account for the lack of a significant change in S : the greater photon capture in normally formed rods would be offset by an increase in A .

Both longer or better organized outer segments, if accompanied by correspondingly greater rhodopsin content, might also serve to mask the expected slowing of dark-adaptation in VCM-treated rats: the time constant of recovery from bleaching (t_{50}) is faster for smaller bleaches (Perlman, 1978).

Future studies of rod structure and of retinal rhodopsin content (e.g., Fulton et al., 1999b) could provide important new evidence as to the effects of VCM on the rods, as could alternative functional techniques such as magnetic resonance imaging (Berkowitz et al., 2009). Overall, the data presented herein are indicative of an advantageous, if transient, effect on rod function in OIR. The transient enhancement of post-receptor function that also seems to have been affected by VCM administration may have resulted from preservation of synaptic connections in the outer plexiform layer, which is attenuated in rat OIR models (Akula et al., 2009; Dorfman et al., 2008), or simply from the preservation of a healthy post-receptor environment, which is dysregulated in OIR (Berkowitz et al., 2007).

Presumably, the altered vascular outcome in VCM-treated rats was consequent to the alteration in retinal function. There is reason to suspect that a change in the metabolic demands of the rods may have underpinned this finding. For one, rods are the most demanding of oxygen of any cell in the body (Cringler et al., 1991; Hagins et al., 1989; Steinberg, 1987) and it is probably no coincidence that the abnormal retinal vasculature that characterizes ROP first appears within the narrow preterm age range when the rods are beginning to develop their light-sensitive outer segments (Provis et al., 1997) and generating a dark current. For another, patients with retinitis pigmentosa (and consequent much decreased rod activity) are protected against vasoproliferative retinopathies (Arden, 2001), as are mice with photoreceptor degenerations (Arden et al., 2005; de Gooyer et al., 2006a,b; Lahdenranta et al., 2001). This has led to the so-called "Arden" hypothesis (Arden et al., 1998, 2005) that exposure to bright light, which attenuates the dark current, will have a beneficial effect on vasoproliferative retinopathy. Indeed, this simple approach of using light to suppress the dark current showed a small beneficial effect

in a pilot study (Fulton et al., 1998). VCM may be a pharmacological similitude of this approach, albeit reducing the metabolic demands of the rods by slowing the visual cycle and outer segment turnover rather than by slowing the constituent current.

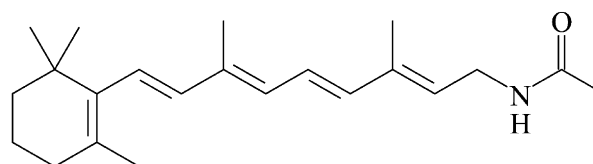
In summary, VCM, an intervention directed at the rod photoreceptor/RPE complex, resulted in transiently altered rod and rod-mediated-post-receptor function and in enhanced recovery of retinal vessel tortuosity in OIR. This is the first demonstration of an effect of systemic treatment with a VCM on a retinopathy in an immature eye. Furthermore, these data represent the first demonstrated causal role for the rod photoreceptors in the development of retinal vasculopathy.

Acknowledgments

We are grateful for the contributions of several people to the generation of data presented in the appendix, Claes Bavik, Ahamd Fawzi and Yang Zhang, and to Ian Scott and Vladimir Kuksa for the chemical data and synthesis.

Appendix

The visual cycle modulator (VCM) used in this study was all-*trans* retinylacetamide, IUPAC: *N*-((2*E*,4*E*,6*E*,8*E*)-3,7-dimethyl-9-(2,6,6-trimethylcyclohex-1-enyl)nona-2,4,6,8-tetraenyl)acetamide; the molecular formula is $C_{22}H_{33}NO$ and the structure is schematized as



The melting point is 131–133 °C (heptane/EtOAc). The compound is moderately susceptible to oxidation and is light-sensitive; it was prepared as a light yellow powder and stored (–80 °C) in individual dark-brown-glass containers under argon that were opened just before every daily injection session. The solubility at 25 °C is <50 ng ml⁻¹ in water and approximately 50 mg ml⁻¹ in ethanol.

Results from preliminary pharmacologic investigations into the action of the compound are described, in brief, below.

In vitro isomerase inhibition: This compound has low *in vitro* isomerization inhibition. Conversion of retinylacetamide to retinylamine *in vivo* is suspected. Both retinylacetamide and retinylamine were tested in a bovine RPE microsome assay (Golczak et al., 2005), and both compounds were found to inhibit the isomerization reaction in a concentration-dependent manner with respective EC₅₀ values of 163 and 0.6 μM.

In vivo isomerase inhibition: An *in vivo* isomerase assay was performed in CD-1 mice (Golczak et al., 2005) and demonstrated that inhibition of recovery was dose-related, with the ED₅₀ estimated at 10–25 mg kg⁻¹ for a single dose and 3–10 mg kg⁻¹ for two weeks of repeated daily dosing. For a single dose, approximately 60% inhibition was achieved with 25 mg kg⁻¹, whereas approximately 90% inhibition was shown after 2-week repeat dosing at 25 mg kg⁻¹ day⁻¹. On the basis of this study, it was concluded that retinylacetamide effectively inhibits murine isomerase activity at doses of 3 mg kg⁻¹ and above in a dose-dependent manner. Maximum inhibition is achieved 16 h after a single dose, and appears to be maintained to 24 h or more after a single dose (Golczak et al., 2005), with a strong accumulative effect after repeat dosing.

Pharmacokinetics: Oral administration of retinylacetamide to rats, dogs and monkeys indicates that administration results in dose-proportional drug-exposure, as assessed by plasma concentrations. Maximal plasma concentrations are achieved 4–8 h after administration, with plasma half-life of approximately 12–16 h. Plasma concentrations following IP injection have not been studied. Retinylacetamide plasma levels increase with repeated dosing, suggesting accumulation.

Toxicology: Toxicological studies in three species (mice, rats and dogs) employed daily oral dosing for up to 28 days. They yielded minimal-to-mild pharmacotoxic findings at higher doses. The “no adverse effect levels” were determined to be 3 mg kg⁻¹ day⁻¹ in both rats and dogs. Findings such as minimal effects on serum enzymes and lipids suggested mild effects on the liver at the highest doses employed (30 mg kg⁻¹ day⁻¹).

References

- Akula, J.D., Favazza, T.L., Mocko, J.A., Benador, I.Y., Asturias, A.L., Kleinman, M.S., Hansen, R.M., Fulton, A.B., 2009. The anatomy of the rat eye with oxygen-induced retinopathy. *Doc. Ophthalmol.*
- Akula, J.D., Hansen, R.M., Martinez-Perez, M.E., Fulton, A.B., 2007. Rod photoreceptor function predicts blood vessel abnormality in retinopathy of prematurity. *Invest. Ophthalmol. Vis. Sci.* 48, 4351–4359.
- Akula, J.D., Mocko, J.A., Benador, I.Y., Hansen, R.M., Favazza, T.L., Vyhovsky, T.C., Fulton, A.B., 2008. The neurovascular relation in oxygen-induced retinopathy. *Mol. Vis.* 14, 2499–2508.
- Alpern, M., Fulton, A.B., Baker, B.N., 1987. “Self-screening” of rhodopsin in rod outer segments. *Vision Res.* 27, 1459–1470.
- Arden, G.B., 2001. The absence of diabetic retinopathy in patients with retinitis pigmentosa: implications for pathophysiology and possible treatment. *Br. J. Ophthalmol.* 85, 366–370.
- Arden, G.B., Sidman, R.L., Arap, W., Schlingemann, R.O., 2005. Spare the rod and spoil the eye. *Br. J. Ophthalmol.* 89, 764–769.
- Arden, G.B., Wolf, J.E., Tsang, Y., 1998. Does dark adaptation exacerbate diabetic retinopathy? Evidence and a linking hypothesis. *Vision Res.* 38, 1723–1729.
- Barnett, J.M., Yanni, S.E., Penn, J.S., 2009. The development of the rat model of retinopathy of prematurity. *Doc. Ophthalmol.*
- Baylor, D.A., Lamb, T.D., Yau, K.W., 1979. Responses of retinal rods to single photons. *J. Physiol.* 288, 613–634.
- Berkowitz, B.A., Roberts, R., Oleske, D.A., Chang, M., Schafer, S., Bissig, D., Gadianu, M., 2009. Quantitative mapping of ion channel regulation by visual cycle activity in rodent photoreceptors in vivo. *Invest. Ophthalmol. Vis. Sci.* 50, 1880–1885.
- Berkowitz, B.A., Roberts, R., Penn, J.S., Gadianu, M., 2007. High-resolution manganese-enhanced MRI of experimental retinopathy of prematurity. *Invest. Ophthalmol. Vis. Sci.* 48, 4733–4740.
- Cringle, S.J., Yu, D.Y., Alder, V.A., 1991. Intraretinal oxygen tension in the rat eye. *Graefes Arch. Clin. Exp. Ophthalmol.* 229, 574–577.
- de Gooyer, T.E., Stevenson, K.A., Humphries, P., Simpson, D.A., Curtis, T.M., Gardiner, T.A., Stitt, A.W., 2006a. Rod photoreceptor loss in Rho^{-/-} mice reduces retinal hypoxia and hypoxia-regulated gene expression. *Invest. Ophthalmol. Vis. Sci.* 47, 5553–5560.
- de Gooyer, T.E., Stevenson, K.A., Humphries, P., Simpson, D.A., Gardiner, T.A., Stitt, A.W., 2006b. Retinopathy is reduced during experimental diabetes in a mouse model of outer retinal degeneration. *Invest. Ophthalmol. Vis. Sci.* 47, 5561–5568.
- Dembinska, O., Rojas, L.M., Chemtob, S., Lachapelle, P., 2002. Evidence for a brief period of enhanced oxygen susceptibility in the rat model of oxygen-induced retinopathy. *Invest. Ophthalmol. Vis. Sci.* 43, 2481–2490.
- Dodt, E., Echte, K., 1961. Dark and light adaptation in pigmented and white rat as measured by electroretinogram threshold. *J. Neurophysiol.* 24, 427–445.
- Dorfman, A., Dembinska, O., Chemtob, S., Lachapelle, P., 2008. Early manifestations of postnatal hyperoxia on the retinal structure and function of the neonatal rat. *Invest. Ophthalmol. Vis. Sci.* 49, 458–466.
- ETROP, 2003. Early Treatment for Retinopathy of Prematurity Cooperative Group. Revised indications for the treatment of retinopathy of prematurity: results of the early treatment for retinopathy of prematurity randomized trial. *Arch. Ophthalmol.* 121, 1684–1694.
- Fulton, A.B., Akula, J.D., Mocko, J.A., Hansen, R.M., Benador, I.Y., Beck, S.C., Fahl, E., Seeliger, M.W., Moskowitz, A., Harris, M.E., 2009a. Retinal degenerative and hypoxic ischemic disease. *Doc. Ophthalmol.* 118, 55–61.
- Fulton, A.B., Baker, B.N., 1984. The relation of retinal sensitivity and rhodopsin in developing rat retina. *Invest. Ophthalmol. Vis. Sci.* 25, 647–651.
- Fulton, A.B., Dodge, J., Hansen, R.M., Schremser, J.L., Williams, T.P., 1991. The quantity of rhodopsin in young human eyes. *Curr. Eye Res.* 10, 977–982.
- Fulton, A.B., Dodge, J., Hansen, R.M., Williams, T.P., 1999a. The rhodopsin content of human eyes. *Invest. Ophthalmol. Vis. Sci.* 40, 1878–1883.
- Fulton, A.B., Hansen, R.M., 1995. Electroretinogram responses and refractive errors in patients with a history of retinopathy prematurity. *Doc. Ophthalmol.* 91, 87–100.
- Fulton, A.B., Hansen, R.M., Findl, O., 1995. The development of the rod photo-response from dark-adapted rats. *Invest. Ophthalmol. Vis. Sci.* 36, 1038–1045.
- Fulton, A.B., Hansen, R.M., Moskowitz, A., Akula, J.D., 2009b. The neurovascular retina in retinopathy of prematurity. *Prog. Retin. Eye Res.*
- Fulton, A.B., Hansen, R.M., Roberto, K., Penn, J.S., 1998. Persistent dysfunction in a rat model of ROP. *Invest. Ophthalmol. Vis. Sci.* 39, S820.
- Fulton, A.B., Reynaud, X., Hansen, R.M., Lemere, C.A., Parker, C., Williams, T.P., 1999b. Rod photoreceptors in infant rats with a history of oxygen exposure. *Invest. Ophthalmol. Vis. Sci.* 40, 168–174.
- Gelman, R., Martinez-Perez, M.E., Vanderveen, D.K., Moskowitz, A., Fulton, A.B., 2005. Diagnosis of plus disease in retinopathy of prematurity using retinal image multiscale analysis. *Invest. Ophthalmol. Vis. Sci.* 46, 4734–4738.
- Golczak, M., Kuksa, V., Maeda, T., Moise, A.R., Palczewski, K., 2005. Positively charged retinoids are potent and selective inhibitors of the trans–cis isomerization in the retinoid (visual) cycle. *Proc. Natl. Acad. Sci. U.S.A.* 102, 8162–8167.
- Good, W.V., 2004. Final results of the Early Treatment for Retinopathy of Prematurity (ETROP) randomized trial. *Trans. Am. Ophthalmol. Soc.* 102, 233–248. discussion 248–250.
- Hagins, W.A., Ross, P.D., Tate, R.L., Yoshikami, S., 1989. Transduction heats in retinal rods: tests of the role of cGMP by pyroelectric calorimetry. *Proc. Natl. Acad. Sci. U.S.A.* 86, 1224–1228.
- Hansen, R.M., Eklund, S.E., Benador, I.Y., Mocko, J.A., Akula, J.D., Liu, Y., Martinez-Perez, M.E., Fulton, A.B., 2008. Retinal degeneration in children: dark adapted visual threshold and arteriolar diameter. *Vis. Res.* 48, 325–331.
- Hartnett, M.E., Martiniuk, D., Byfield, G., Geisen, P., Zeng, G., Bautch, V.L., 2008. Neutralizing VEGF decreases tortuosity and alters endothelial cell division orientation in arterioles and veins in a rat model of ROP: relevance to plus disease. *Invest. Ophthalmol. Vis. Sci.* 49, 3107–3114.
- Hood, D.C., Birch, D.G., 1992. A computational model of the amplitude and implicit time of the b-wave of the human ERG. *Vis. Neurosci.* 8, 107–126.
- Howes, K.A., Pennesi, M.E., Sokal, I., Church-Kopish, J., Schmidt, B., Margolis, D., Frederick, J.M., Rieke, F., Palczewski, K., Wu, S.M., Detwiler, P.B., Baehr, W., 2002. GCAP1 rescues rod photoreceptor response in GCAP1/GCAP2 knock-out mice. *EMBO J.* 21, 1545–1554.
- Hughes, A., 1979. A schematic eye for the rat. *Vision Res.* 19, 569–588.
- Kuksa, V., Imanishi, Y., Batten, M., Palczewski, K., Moise, A.R., 2003. Retinoid cycle in the vertebrate retina: experimental approaches and mechanisms of isomerization. *Vision Res.* 43, 2959–2981.
- Lahdenranta, J., Pasqualini, R., Schlingemann, R.O., Hagedorn, M., Stallcup, W.B., Bucana, C.D., Sidman, R.L., Arap, W., 2001. An anti-angiogenic state in mice and humans with retinal photoreceptor cell degeneration. *Proc. Natl. Acad. Sci. U.S.A.* 98, 10368–10373.
- Lamb, T.D., Pugh Jr., E.N., 1992. A quantitative account of the activation steps involved in phototransduction in amphibian photoreceptors. *J. Physiol.* 449, 719–758.
- Liu, K., Akula, J.D., Falk, C., Hansen, R.M., Fulton, A.B., 2006. The retinal vasculature and function of the neural retina in a rat model of retinopathy of prematurity. *Invest. Ophthalmol. Vis. Sci.* 47, 2639–2647.
- Lutty, G.A., Chan-Ling, T., Phelps, D.L., Adamis, A.P., Berns, K.I., Chan, C.K., Cole, C.H., D’Amore, P.A., Das, A., Deng, W.T., Dobson, V., Flynn, J.T., Friedlander, M., Fulton, A., Good, W.V., Grant, M.B., Hansen, R., Hauswirth, W.W., Hardy, R.J., Hinton, D.R., Hughes, S., McLeod, D.S., Palmer, E.A., Patz, A., Penn, J.S., Raisler, B.J., Repka, M.X., Saint-Geniez, M., Shaw, L.C., Shima, D.T., Smith, B.T., Smith, L.E., Tahija, S.G., Tasman, W., Trese, M.T., 2006. Proceedings of the Third International Symposium on Retinopathy of Prematurity: an update on ROP from the lab to the nursery (November 2003, Anaheim, California). *Mol. Vis.* 12, 532–580.
- Lyubarsky, A.L., Pugh Jr., E.N., 1996. Recovery phase of the murine rod photo-response reconstructed from electroretinographic recordings. *J. Neurosci.* 16, 564–571.
- Lyubarsky, A., Nikonov, S., Pugh Jr., E.N., 1996. The kinetics of inactivation of the rod phototransduction cascade with constant Ca²⁺. *J. Gen. Physiol.* 107, 19–34.
- Martinez-Perez, M.E., Hughes, A.D., Stanton, A.V., Thom, S.A., Chapman, N., Bharath, A.A., Parker, K.H., 2002. Retinal vascular tree morphology: a semi-automatic quantification. *IEEE Trans. Biomed. Eng.* 49, 912–917.
- Martinez-Perez, M.E., Hughes, A.D., Thom, S.A., Bharath, A.A., Parker, K.H., 2007. Segmentation of blood vessels from red-free and fluorescein retinal images. *Med. Image Anal.* 11, 47–61.
- Matthews, H.R., Fain, G.L., 2003. The effect of light on outer segment calcium in salamander rods. *J. Physiol.* 552, 763–776.
- McBee, J.K., Palczewski, K., Baehr, W., Pepperberg, D.R., 2001. Confronting complexity: the interlink of phototransduction and retinoid metabolism in the vertebrate retina. *Prog. Retin. Eye Res.* 20, 469–529.
- Messias, A., Zrenner, E., Tzekov, R., McGee, D., Peters, T., Wilhelm, B., Baryluk, A., Kubota, R., Gekeler, F., 2010. Single doses of all-trans-N-retinylacetamide slow down the ERG amplitude recovery after bleaching in rats. *Doc. Ophthalmol.* 120, 165–174.
- Moiseyev, G., Chen, Y., Takahashi, Y., Wu, B.X., Ma, J.X., 2005. RPE65 is the isomero-hydrolase in the retinoid visual cycle. *Proc. Natl. Acad. Sci. U.S.A.* 102, 12413–12418.
- Palmer, E.A., Flynn, J.T., Hardy, R.J., Phelps, D.L., Phillips, C.L., Schaffer, D.B., Tung, B., 1991. Incidence and early course of retinopathy of prematurity. The cryotherapy

- for retinopathy of prematurity cooperative group. *Ophthalmology* 98, 1628–1640.
- Pe'er, J., Shweiki, D., Itin, A., Hemo, I., Gnessin, H., Keshet, E., 1995. Hypoxia-induced expression of vascular endothelial growth factor by retinal cells is a common factor in neovascularizing ocular diseases. *Lab Invest.* 72, 638–645.
- Penn, J.S., Henry, M.M., Tolman, B.L., 1994. Exposure to alternating hypoxia and hyperoxia causes severe proliferative retinopathy in the newborn rat. *Pediatr. Res.* 36, 724–731.
- Penn, J.S., Henry, M.M., Wall, P.T., Tolman, B.L., 1995. The range of PaO₂ variation determines the severity of oxygen-induced retinopathy in newborn rats. *Invest. Ophthalmol. Vis. Sci.* 36, 2063–2070.
- Perlman, I., 1978. Kinetics of bleaching and regeneration of rhodopsin in abnormal (RCS) and normal albino rats in vivo. *J. Physiol.* 278, 141–159.
- Provis, J.M., Leech, J., Diaz, C.M., Penfold, P.L., Stone, J., Keshet, E., 1997. Development of the human retinal vasculature: cellular relations and VEGF expression. *Exp. Eye Res.* 65, 555–568.
- Pugh Jr., E.N., Lamb, T.D., 1993. Amplification and kinetics of the activation steps in phototransduction. *Biochim. Biophys. Acta* 1141, 111–149.
- Rando, R.R., 2001. The biochemistry of the visual cycle. *Chem. Rev.* 101, 1881–1896.
- Reiser, M.A., Williams, T.P., Pugh Jr., E.N., 1996. The effect of light history on the aspartate-isolated fast-PIII responses of the albino rat retina. *Invest. Ophthalmol. Vis. Sci.* 37, 221–229.
- Reynaud, X., Dorey, C.K., 1994. Extraretinal neovascularization induced by hypoxic episodes in the neonatal rat. *Invest. Ophthalmol. Vis. Sci.* 35, 3169–3177.
- Reynaud, X., Hansen, R.M., Fulton, A.B., 1995. Effect of prior oxygen exposure on the electroretinographic responses of infant rats. *Invest. Ophthalmol. Vis. Sci.* 36, 2071–2079.
- Shweiki, D., Itin, A., Soffer, D., Keshet, E., 1992. Vascular endothelial growth factor induced by hypoxia may mediate hypoxia-initiated angiogenesis. *Nature* 359, 843–845.
- Sieving, P.A., Chaudhry, P., Kondo, M., Provenzano, M., Wu, D., Carlson, T.J., Bush, R. A., Thompson, D.A., 2001. Inhibition of the visual cycle in vivo by 13-cis retinoic acid protects from light damage and provides a mechanism for night blindness in isotretinoin therapy. *PNAS USA* 94, 1835–1840.
- Steinberg, R., 1987. Monitoring communications between photoreceptors and pigment epithelial cells: effects of “mild” systemic hypoxia. *Invest. Ophthalmol. Vis. Sci.* 28, 1888–1903.
- Travis, G.H., Golczak, M., Moise, A.R., Palczewski, K., 2007. Diseases caused by defects in the visual cycle: retinoids as potential therapeutic agents. *Annu. Rev. Pharmacol. Toxicol.* 47, 469–512.
- Tsai, T.I., Bui, B.V., Vingrys, A.J., 2009. Dimethyl sulphoxide dose–response on rat retinal function. *Doc. Ophthalmol.* 119, 199–207.
- Wellard, J., Lee, D., Valter, K., Stone, J., 2005. Photoreceptors in the rat retina are specifically vulnerable to both hypoxia and hyperoxia. *Vis. Neurosci.* 22, 501–507.
- Whitmore, G.A., 1986. Prediction limits for a univariate normal observation. *Am. Stat.* 40, 141–143.
- Wyszecki, G., Stiles, W.S., 1982. *Color Science: Concepts and Methods, Quantitative Data and Formulae*. Wiley, New York.
- Young, R.W., 1967. The renewal of photoreceptor cell outer segments. *J. Cell Biol.* 33, 61–72.